The Estimation and Evaluation of Shoreline Locations, Shoreline-Change Rates, and Coastal Volume Changes Derived from Landsat Images

Do, Anh T.K.; De Vries, Sierd; Stive, Marcel J.F.

DOI
10.2112/JCOASTRES-D-18-00021.1

Publication date
2019

Document Version
Final published version

Published in
Journal of Coastal Research

Citation (APA)
Do, A. T. K., De Vries, S., & Stive, M. J. F. (2019). The Estimation and Evaluation of Shoreline Locations, Shoreline-Change Rates, and Coastal Volume Changes Derived from Landsat Images. *Journal of Coastal Research*, *35*(1), 56-71. https://doi.org/10.2112/JCOASTRES-D-18-00021.1

Journal of Coastal Research	35	1	56–71	Coconut Creek, Florida	January 2019

The Estimation and Evaluation of Shoreline Locations, Shoreline-Change Rates, and Coastal Volume Changes Derived from Landsat Images

Anh T.K. Do[†‡], Sierd de Vries[†], and Marcel J.F. Stive[†]*

[†]Faculty of Civil Engineering and Geosciences
Delft University of Technology
Delft, The Netherlands

[‡]Faculty of Water Resources Engineering
University of Da Nang (UD) - University of Science and Technology (DUT)
Da Nang, Viet Nam

www.cerf-jcr.org

www.JCRonline.org

ABSTRACT

Do, A.T.K.; de Vries, S., and Stive, M.J.F., 2019. The estimation and evaluation of shoreline locations, shoreline-change rates, and coastal volume changes derived from Landsat images. *Journal of Coastal Research,* 35(1), 56–71. Coconut Creek (Florida), ISSN 0749-0208.

Shoreline-change data are of primary importance for understanding coastal erosion and deposition as well as for studying coastal morphodynamics. Shoreline extraction from satellite images has been used as a low-cost alternative and as an addition to traditional methods. In this work, satellite-derived shorelines and corresponding shoreline-change rates and changes in volumes of coastal sediments have been estimated and evaluated for the case of the data-rich North-Holland coast. This coast is globally unique for its long *in situ* monitoring record and provides a perfect case to evaluate the potential of shoreline mapping techniques. A total of 13 Landsat images and 233 observed cross-shore profiles (from the JAaRlijkse KUStmeting [JARKUS] database) between 1985 and 2010 have been used in this study. Satellite-derived shorelines are found to be biased in seaward direction relative to the JARKUS-derived shorelines, with an average ranging 8 m to 9 m over 25 years. Shoreline-change rates have been estimated using time series of satellite-derived shorelines and applying linear regression. The satellite-derived shoreline-change rates show a high correlation coefficient ($R^2 > 0.78$) when compared with the JARKUS-derived shoreline-change rates over a period of 20 and 25 years. Volume changes were calculated from the satellite-derived shoreline-change rates using assumptions defining a closure depth. Satellite-derived volume changes also show a good agreement with JARKUS-based values. Satellite-derived shorelines compare better with *in situ* data on beaches that have intertidal zone widths ranging from one- to two-pixel sizes (30 m–60 m). The results show that the use of Landsat images for deriving shorelines, shoreline-change rates, and volume changes have accuracies comparable to observed JARKUS-based values when considering decadal scales of measurements. This shows the potential of applying Landsat images to monitor shoreline change and coastal volume change over decades.

ADDITIONAL INDEX WORDS: *Landsat images, shoreline-change rate, shoreline-position uncertainty, coastal volume changes*.

INTRODUCTION

Monitoring the behavior of shorelines is of considerable social and economic importance in support of setback planning, hazard zoning, erosion-accretion management, regional sediment budgets, and the establishment and validation of models for coastline changes (Lawrence, 1994; Sherman and Bauer, 1993; Zuzek, Nairn, and Thieme, 2003). Shorelines are inherently dynamic features that mark the transition zone between land and sea. The inherent dynamics of the shoreline span over a range of spatial and temporal scales (Gens, 2010; Pajak and Leatherman, 2002), which makes shoreline-change assessment very challenging. The zone around the shoreline is highly dynamic and undergoes frequent changes caused by the impact of both natural and human activities. Furthermore, shoreline erosion and coastal flooding are highlighted as among the largest effects of climate change (IPCC, 2001).

Traditional techniques for shoreline-change studies include analyzing historic maps, *in situ* beach profiling, LIDAR surveys, and aerial photography and video imagery (Chen and Chang, 2009; Kumar and Jayappa, 2009; Miller and Fletcher, 2003; Pianca, Holman, and Siegle, 2015; Ruggiero *et al*., 2005). These techniques are inherently limited in temporal coverage, typically being either too short to identify long-term trends or too widely spaced in time to distinguish short-term, seasonal changes. Also, traditional techniques are both costly and labor intensive. For developing countries, budgets for coastal monitoring and shoreline change are scarce. Therefore, a cost-effective approach is required, particularly for those places where there is concern about shoreline erosion. This is where satellite imagery based on freely available high-quality images such as Landsat might offer a good alternative. Moreover, it is possible to assess coastline changes over longer periods of time since Landsat missions have been collecting spectral satellite imagery for over 40 years now (Guariglia *et al*., 2006; Maiti and Bhattacharya, 2009).

Satellite-derived shoreline (SDS) is based on extracting shorelines from collected satellite images based on grouping pixels by their different spectral properties in different wavebands (*e.g.,* Lu and Weng, 2007; Muttitanon and Tripathi, 2005; Phinn *et al*., 2000). These methods have been widely used in recent decades for automatic and semiautomatic shoreline detection and mapping. Some studies use a single band image (Frazier and Page, 2000), while other studies use a band ratio

DOI: 10.2112/JCOASTRES-D-18-00021.1 received 19 February 2018; accepted in revision 24 July 2018; corrected proofs received 14 September 2018; published pre-print online 17 October 2018.
*Corresponding author: m.j.f.stive@tudelft.nl

(Guariglia *et al*., 2006) or a combination of different reflective bands to improve surface water detection (Du *et al*., 2012). For instance, the Normalized Difference Water Index (McFeeters, 1996) was used to enhance the difference in pixel resolution between land and water in shoreline extraction (Bouchahma and Yan, 2012; Grigio *et al*., 2005; Noernberg and Marone, 2003). Also, the Normalized Difference Moisture Index (Wilson and Sader, 2002), the Modified Normalized Difference Water Index (Xu, 2006), the Water Ratio Index (Shen and Li, 2010), the Normalized Difference Vegetation Index (Rouse *et al*., 1974), and the Automated Water Extraction Index (Feyisa *et al*., 2014) also found wide application. Rokni *et al*. (2014) applied and compared the different previous satellite-derived indexes to extract surface water of Lake Urmia. Their results demonstrated that the Normalized Difference Water Index (NDWI) is superior to other indexes with the highest accuracy results. Consequently, NDWI was selected as the method to extract shoreline positions in this study. More recently, new approaches for shoreline extraction have been investigated. Foody, Muslim, and Atkinson (2003); Muslim, Foody, and Atkinson (2006); and Pardo-Pascual *et al*. (2012) explore subpixel shoreline extraction in which individual pixels could be assigned to partly land and partly water.

Many previous studies have investigated the potential of optical satellite images for coastal monitoring (Blodget, Taylor, and Roark, 1991; Chen and Chang, 2009; Dinesh Kumar *et al*., 2007; Ekercin, 2007; Elena, 2008; Foody, Muslim, and Atkinson 2003; Gutierres *et al*., 2016; Kingston, 2003; Kuleli *et al*., 2011; Liu and Jezek, 2004; Mason, Davenport, and Flather, 1997; Plant *et al*., 2007; Teodoro, 2016; Teodoro *et al*., 2018; Wang, Zhang, and Ma, 2010; White and El-Asmar, 1999). However, few of these studies have fully explored the accuracy of the derived shorelines through comparison with simultaneous and independent *in situ* observations because of limitations in the availability of satellite images and *in situ* data.

A literature search resulted in only five recent studies related to SDS accuracy. First, Pardo-Pascual *et al*. (2012) used 45 images (28 TM and 17 ETM) to assess accuracy in shoreline position extraction applying the subpixel method with two shoreline segments comprising seawalls in the Spanish Mediterranean Sea. This case applies only to artificially stabilized coastal segments that have a constant shoreline position. Moreover, the accuracy was derived by using only one reference image; however, on natural beaches the shoreline positions are variable because of seasonal and episodic events. For this reason, the accuracy assessment for seawalls is not the same as for natural beaches. Second, García-Rubio, Huntley, and Russell (2015) used *in situ* shoreline measurements to compare with SDS from multispectral images (SPOT) with eight shoreline segments, including a beach and a man-made structure at Progreso, Yucatá, México. Again, their research used only one image to evaluate accuracy. Third, Almoncaid-Caballer *et al*. (2016) used the annual mean shoreline positions (the average shoreline position over a year) extracted from Landsat images to quantify the mid-term beach trend during the period of 2000–14. In their work, the annual mean Landsat shorelines were compared with the mean annual shorelines obtained from more accurate sources RTK-GPS and LIDAR. The test was applied on a 9 km stretch of beach at El Saler (Valencia, Spain) located on the beach barrier. It is shown that the use of annual mean shorelines indicates that the same rate of change is obtained as when using the whole set of shorelines. Both instantaneous and mean annual shorelines appear to show a seaward bias of about 4 or 5 m compared to those obtained using LIDAR and RTK-GPS. Similarly, Sánchez-García *et al*. (2015) also used the same method for extraction shoreline position, as described in Pardo-Pascual *et al*. (2012) to compare an annual mean shoreline obtained from Landsat TM /ETM+ and from high precision data, RTK-GPS. The comparison was applied on a 9-km stretch of beach at El Saler (Valencia, Spain) for two short periods (2006–07 and 2009–10). Several statistical tests were performed to compare the grade of similarity between Landsat and high-precision data, which indicates that both sources of data provide similar information regarding annual mean shoreline. Finally, Hagenaars *et al*. (2018) have evaluated different drivers of inaccuracy of SDS using very detailed measurements of morphology. Their results contain a near perfect comparison of SDS and *in situ* data that were collected simultaneously during cloud-free conditions showing an average accuracy of about 1 m.

No previous studies have explored the potential of deriving changes in coastal volumes using satellite data. Only Rosati, Gravens, and Smith (1999) used 10 historical shoreline data sets from survey maps, aerial photography, and digital rectified scanned aerial photography to estimate volumetric-change rates to derive a regional sediment budget for Fire Island to Montauk Point. These authors focused on the time period from 1979 to 1995 (a 16-year time period). Their research considered only general uncertainties in their regional sediment-budget estimation based on the potential longshore sediment transport (LST). The uncertainty was derived following Kraus and Rosati (1998), who divided the standard deviation (SD) in the net LST by the square root of the number of yearly averages. This evaluation did not use any observed data for validation.

The aim of the present study is to explore the potential of satellite images in monitoring shoreline-change rates and changes in volumes of coastal sediments that can be applied to beach locations where data are lacking or scarce. Specific objectives are to provide a straightforward, quantitative, and objective method that builds on existing methods that have proven to be easy and widely applicable for extracting shoreline locations using satellite images. The estimation of shoreline-change rates follows this derivation of shoreline position and eventually changes in coastal sediment volumes. These processes were applied and evaluated at the Dutch coast, which provides a data-rich site to evaluate the methodology.

Study Site

The selected study area is located at the North-Holland coast and stretches from Wijk aan Zee to Den Helder, over a length of approximately 60 km (Figure 1). It is bounded in the north by a tidal inlet (the Marsdiep) and in the south by the 2.5-km long jetties of IJmuiden. The North-Holland coast is a sandy, microtidal, wave-dominated coast. The plan shape of the coast is slightly concave, except near the Petten Seawall that protrudes into the sea, giving the shoreline a local convex curvature. The coastline orientation in the north is about 2° with respect to the north and increases up to 22° at IJmuiden.

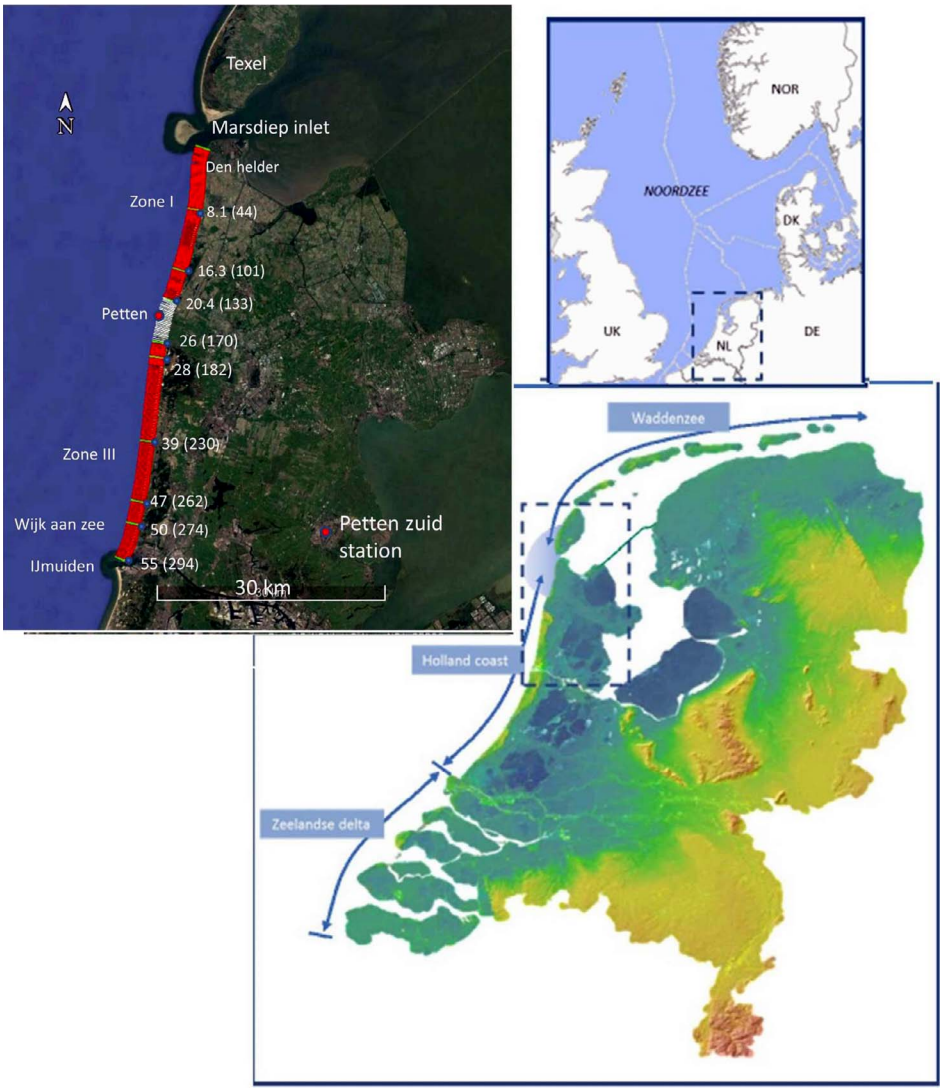

Figure 1. Overview of The Netherlands, its three coastal systems, and the study area (modified from Actueel Hoogtebestand Nederland, 2010). (Color for this figure is available in the online version of this article.)

The average beach slope is in the order of 1:60. The near shore zone has an average slope of 1:60–1:150 (Knoester, 1990). The slopes can vary significantly in longshore direction. Near Den Helder, the influence of the channels of the Marsdiep inlet cause steeper slopes. Near IJmuiden, the dry beach and the near shore zone have a larger width. Most of the winds along the Holland coast come from the North Sea. The prevailing wind direction is SW (23%), followed by west (16%), east (13%), and NW (12%) (Stolk, 1989). Storms that cause the largest wind setup along the coast are coming from NW (van Rijn, Ruessink, and Mulder, 2002). Tides are semidiurnal with a mean tidal range between 1.4 m in the north and 1.6 m in the south. Waves mainly approach the coast from SW and NNW directions. The wave climate is quite homogeneous along the whole stretch of coast (Wijnberg, 2002), with a mean annual significant wave height of about 1.3 m.

Landsat Images

To detect SDS of the North-Holland coast, a total of 13 Landsat images were selected with the lowest cloud coverage. All the used images are free of clouds, except Landsat TM, 2 October 1988 (10% cloud coverage), and Landsat TM, 2 June 2010 (8% cloud coverage). The availability of cloud-free images did not allow a subset of images at regular intervals. Thirty scenes of the Thematic Mapper (Landsat 5 TM) and Enhanced Thematic Mapper (Landsat 7 ETM+) sensor data were acquired during the period from 1985 to 2010. Those were downloaded from the U.S. Geological Survey (USGS) Earth Explorer Web Tool. All the obtained Landsat data (Level 1 Terrain Corrected [L1T] product) were pregeoreferenced to UTM zone 31 North projection using WGS-84 datum. Landsat 5 TM comprises seven spectral bands with a spatial resolution of 30 m for bands 1 to 5 and 7, and one thermal band (band 6) is 120 m that is resampled

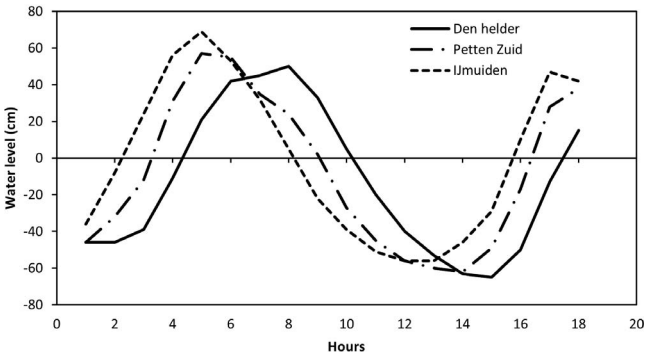

Figure 2. The difference in the tide between the stations, Den Helder, Petten Zuid, and IJmuiden.

to 30-m pixels. Landsat 7 ETM+ comprises eight spectral bands with a spatial resolution of 30 m for bands 1 to 7. The resolution of band 8 (panchromatic) is 15 m. As reported by the National Aeronautics and Space Administration, all the Landsat TM/ETM+ are georeferenced with a level of precision better than 0.44 pixels (meaning 13.4 m) (Pardo-Pascual *et al.,* 2012).

For the interpretation of the satellite dataset, it is important to take the instantaneous water level into account. The observed location of the waterline is influenced by the instantaneous water level where a change of water level by 1 m will cause the waterline to shift 50 m over a 1:50 beach slope when other factors are assumed constant. Instantaneous water levels are measured at several locations in the study area. Along the study area, there are three tidal stations; Den Helder, Petten Zuid, and IJmuiden. The tide station of Den Helder is located in the tidal inlet and is thus not necessarily representative for tide level along the coast (Wijnberg, 2002). The tide station of IJmuiden is located near the IJmuiden harbor. Figure 2 indicates one tidal cycle in January 1985 at the three tidal stations. There is a slight difference in phase and tidal ranges between the stations. The tidal range indicates a slight increase from Den Helder to I IJmuiden. To identify how tides influence the SDS, a numerical model must be applied to simulate the tidal wave propagation along the coast, but this falls beyond the scope of this study. The Petten Zuid station is located near the Petten seawall, in the middle of Noord Holland. The tide measured at the Petten Zuid station was therefore selected as representative for the study area because it is the closest to the study area. The tidal conditions at the time of image acquisition were estimated by the tide data at Petten Zuid station (Live Waterbase, 2018). The tide level corresponding to the moment of the Landsat image collection is presented in Table 1 alongside the details of the satellite data.

JAaRlijkse KUStmeting (JARKUS) Data

To assess the accuracy of SDS, shoreline positions were derived from the JARKUS database available for this study (Minneboo, 1995). A yearly survey program for the Dutch coastal area collects the JARKUS profile data since 1963. Long fixed transects at a longshore distance of 200 m–250 m, depths, and heights of coastal profiles are measured each year, called JARKUS profiles. These data are primarily used to inspect and provide the position of the momentary coastline, to record volumes of beach profiles and to plan nourishments. Because of the size of the JARKUS data, they are grouped into 16 regions covering the Dutch North Sea coast from North to South. This study used the data of region 7 (Noord-Holland), which includes 294 transects (corresponding to the name of profile in JARKUS data, 7000000 to 7005500) locations in total covering the coast from Den Helder to Wijk aan Zee.

Because of its geography, the North-Holland coast was divided into three segments for the analysis. The first segment, termed Zone I, is located immediately south of the Marsdiep inlet starting from transect 2 to transect 133. The second segment, termed Zone II, includes 31 transects from transect 134 to transect 170. This segment is located at the Petten seawall, where JARKUS profile data are available only since 1990. The third segment is Zone III, starting from transect 171 to transect 294 at the jetties of IJmuiden. Landsat-derived shorelines along seawalls are not necessarily the same as along natural shorelines (Almonacid-Caballer *et al*., 2016). On a seawall stretch, the water depth close to the shoreline increases sharply, whereas on natural beaches the depth drops more gradually. As a result, the shoreline definition is different; therefore, this study focuses only on the accuracy assessment for natural beaches, Zone I and Zone III.

METHODS

To assess the accuracy of using satellite images in monitoring shoreline-change rates and changes in coastal volume, the

Table 1. *Details of the satellite dataset used in this study.*

No	Path/Row	Acq. Date	Acq. Time	Sensor	Tidal Height (cm)
1	199/23	12 February 1985	10:10:04	TM	34
2	198/23	16 June 1986	9:57:10	TM	65
3	198/23	05 July 1987	9:58:26	TM	67
4	199/23	02 October 1988	10:10:16	TM	47
5	199/23	23 May 1989	10:01:51	TM	12
6	199/23	30 March 1990	9:59:43	TM	6
7	198/23	16 May 1998	10:10:54	TM	29
8	198/23	30 July 1999	10:26:20	ETM	7
9	198/23	13 May 2000	10:25:34	ETM	−24
10	198/23	08 September 2005	10:21:34	TM	50
11	198/23	11 September 2006	10:27:11	TM	69
12	198/23	19 September 2009	10:23:16	TM	−31
13	198/23	02 June 2010	10:24:09	TM	58

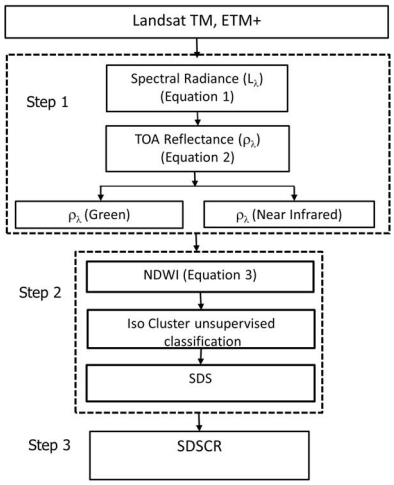

Figure 3. Flow chart of shoreline-change analysis methodology.

present work used the most common and easy-to-apply method as the basic method to derive shoreline position (SDS). Then SDR change rates (SDSCR) are calculated based on the SDS and the volume changes (SDVC) are estimated based on the SDSCR. Additionally, shoreline positions, shoreline-change rates and volume changes derived from JARKUS data are used to access accuracy by using statistical parameters.

Extracting SDSs from Landsat Images

The SDS is defined as the position of the boundary between water and land at the time of satellite imagery acquisition. To detect the shoreline position and to calculate the shoreline-change rate, this study applied an algorithm, as shown in the flow chart in Figure 3 comprising three main steps. (1) Conversion of the digital number (DN) to spectral radiance (L_λ) and to the top of atmospheric (TOA) reflectance (ρ_λ) for radiometric calibration according to Chander, Markham, and Helder (2009); this step is applied for two bands: the green and near infrared bands. (2) Extracting SDS based on classification of the NDWI values by using unsupervised classification techniques. (3) All shoreline positions were used to derive shoreline-change rates.

Step 1 comprises radiometric calibration and atmospheric correction. Data records of different remote sensors are not directly comparable because time differences occur in image acquisition, signal variations of exoatmostpheric solar irradiance arise from spectral band distinctions, and atmospheric effects of aerosol scattering under various weather conditions on the image acquisition date occur (Kuleli *et al*., 2011). Therefore, it is necessary to conduct radiometric calibration and to apply atmospheric correction before extracting the shoreline position (Chander, Markham, and Helder, 2009; Tyagi and Bhosle, 2011). The DNs recorded by the Landsat TM and ETM+ were transformed to TOA reflectance (ρ_λ) using the method developed by Chander, Markham, and Helder (2009). During radiance calibration, the DNs recorded by Landsat images were converted to radiance values (L_λ) using the bias and gain values following Equation (1). Then these radiance values were converted to reflectance values using Equation (2):

$$L_\lambda = G_{rescale} \times Q_{cal} + B_{rescale} \quad (1)$$

and

$$\rho_\lambda = \frac{\pi \cdot L_\lambda \cdot d^2}{ESUN_\lambda \cdot \sin\theta_{SE}} \quad (2)$$

where, L_λ = spectral radiance at the sensor's aperture [W/(m^2 sr μm)], Q_{cal} = quantized calibrated pixel value (DN), G_{rescale} = band-specific rescaling gain factor [(W/(m^2 sr μm))/DN], B_{rescale} = band-specific rescaling bias factor [(W/(m^2 sr μm)/DN], ρ_λ = planetary TOA reflectance (dimensionless), d = earth-sun distance [astronomical units], ESUN_λ = mean exoatmospheric solar irradiance [W/(m^2 μm)], and θ_{SE} = local sun-elevation angle.

Step 2 involves extracting the SDS based on the classification of the NDWI values. To enhance maximum distinction between land and sea, the NDWI was used according to Equation (3) (McFeeters, 1996):

$$\text{NDWI} = (\rho_\lambda(\text{Green}) - \rho_\lambda(NIR))/(\rho_\lambda(\text{Green}) + \rho_\lambda(NIR)) \quad (3)$$

where, Green is the green band (Land sat TM/ETM+ band 2), and NIR is the near infrared band (Land sat TM/ETM+ band 4). The NDWI is designed to (1) maximize reflectance of water using green wave lengths, (2) minimize the low reflectance of NIR by water features, and (3) take advantage of the high reflectance of NIR by vegetation and soil features. As a result, water features have positive and enhanced values, while vegetation and soil usually have zero or negative values and are therefore suppressed (McFeeters, 1996). Moreover, the NDWI technology can avoid the influence of the water content of leaves of vegetation and the influence of floating leaved vegetation and extract the pure standing-water content (Karsli, Guneroglu, and Dihkan, 2011). The unsupervised classification by the Iterative Self-Organizing Data Analysis Technique Algorithm (ISODATA) method was applied to identify pixels as sea and land. This method does not require information about the image while classification and is therefore especially useful in data-poor cases compared to other algorithms. The ISODATA method requires the user to set thresholds for different classification parameters. Liu *et al*. (2011) advise consideration of higher numbers of classes for coastal areas of many different land covers and lower classes for areas comprising only few types of land cover. Because this paper's study zone is a long stretch of coast and the images' region covers different types of land cover, 20 classes were needed to define land and water surface appropriately. A lower and a higher number of classes resulted in either a poor description of land and water surface or a poor distinction because some classes can be merged or removed. The process of the classification from the NDWI images is including the intermediate steps mentioned illustrated in Figure 4. The shoreline identification is based on grouping all classified pixels from the NDWI image, from 20 classes, into two contrasting classes, water and land. The output from the classification process is an image with pixels grouped either as sea or land. The boundary between land

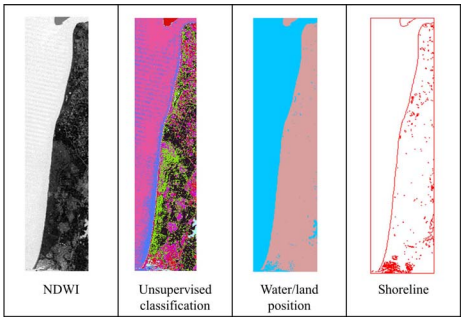

Figure 4. Processing to extract shoreline position from Landsat (example data of 2005). (Color for this figure is available in the online version of this article.)

and sea in the classified image is converted into a vector. The resulting vector requires a manual edit whereby inland features not related to the shoreline are removed. The process of extracting the shoreline position is performed using the ArcGIS 10.2 software suite (ESRI, 2014).

Step 3 involves the derivation of the SDSCR by using linear regression. This method is available in the Digital Shoreline Analysis System (DSAS) software version 4.3, an ArcGIS extension for calculating shoreline change developed by the USGS (Thieler *et al*., 2009). A baseline is constructed to serve as a starting point for all transects derived by the DSAS application. The transects used are at the same locations as the JARKUS data to allow for comparison. A least-squares regression line is fitted to all shoreline points for a particular transect (Thieler *et al*., 2009). The evaluation of SDSCR are performed over a 5-year period (1985–90), two 10-year periods (1990–2000, 2000–10), a 20-year period (1990–2010), and a 25-year period (1985–2010).

Observed Shoreline Position from JARKUS Profiles

To extract shorelines from JARKUS profiles, the measured water level at Petten Zuid tidal station was used to find the intersection point between the water level and the cross-shore profiles corresponding to the time appearances of the Landsat images. The water level corresponding to each Landsat image was derived using the exact date and time of image collection. The location of the observed shoreline position from JARKUS is derived as the intersection between each of the 294 cross-shore profiles and the water level at the time of Landsat image collection.

Calculation of Profile Volumes from Satellite and JARKUS Data

The SDVC for each transect, ΔV_{SDS} (m^3/y), was calculated from the shoreline-change rates by assuming that the shoreline is translated horizontally without changing shape over an active depth (A_D), as shown in Figure 5. This is summarized in Equation (4) (Rosati, 2005; Rosati and Kraus, 1999):

$$\Delta V_{SDS} = A_D \Delta_y \Delta_x \tag{4}$$

where, Δy is the shoreline-change rate for each transect (m/y), A_D is the active depth for each transect (m), and Δx represents the transect spacing (m). The active depth represents the

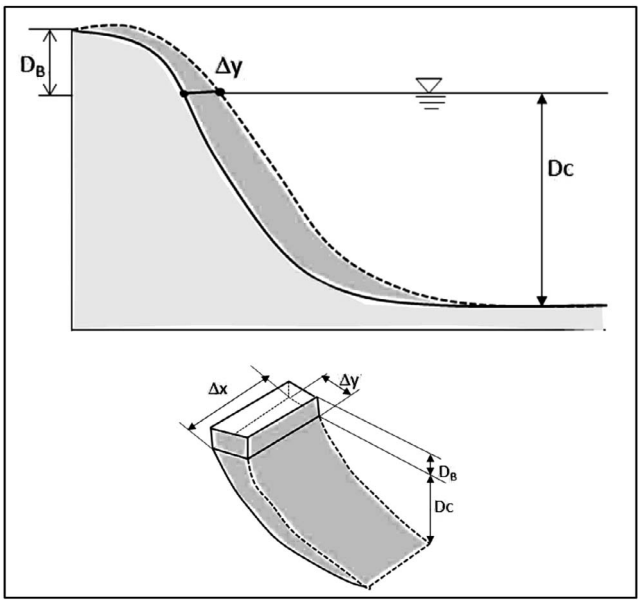

Figure 5. Assumption volume calculated from SDS.

vertical extent of the beach profile that is eroding or accreting during the period of consideration. It is typically defined as the absolute sum of the berm crest or dune elevation, D_B, and depth of closure, D_c (Equation [5]):

$$A_D = D_B + D_c. \tag{5}$$

The volume change for each transect derived from the JARKUS profiles, $\Delta V_{\mathrm{profile}}$ (m^3/y), was estimated using linear regression. First, the volume of each transect of each year, $\Delta V_{\mathrm{profile}}$ (m^3/m), was derived based on the JARKUS profile. The dune elevation (D_B) was used as the landward boundary, and the closure depth, D_c, was used as the seaward limit for this volume calculation (Figure 6). Then the volume change in (m^3/m) was estimated by multiplying with the transect distance, Δx (m) to have the total volume change in (m^3). After that, the volume change of each transect, $\Delta V_{\mathrm{profile}}$ (m^3/y), over a period was estimated by fitting a least squares regression line to the yearly volume trends.

In Figure 6, the dune elevation (D_B) is shown as the highest point of the profile. The depth of closure (D_c) can be estimated using measurements of the active beach profiles if this data is available or by using the analytical method proposed by Hallermeier (1978). In this study at the Dutch coast, the closure depth parameter is taken from literature Hinton and Nicholls (1998). Therefore, a value of the closure depth of 8 m for the area of North-Holland is assumed. In case the measured profiles do not extend to the 8 m depth contour, the seaward limit is set to the most seaward measurements in that profile.

To compare the volume changes, ΔV_{SDS} (m^3/y) and $\Delta V_{\mathrm{profile}}$ (m^3/y) values were derived for different periods. A 5-year period (1985–90), two 10-year periods (1990–2000, 2000–10), a 20-year period (1990–2010), and a 25-year period (1985–2010) were considered.

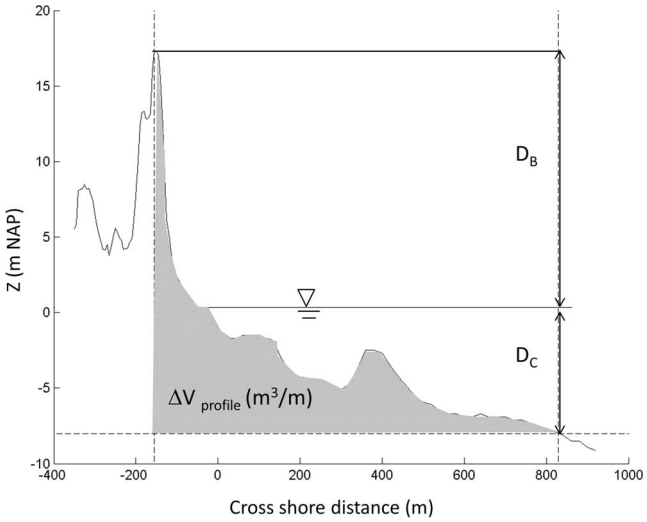

Figure 6. Volume derived from JARKUS profile (transect 235 in year 1985).

Besides presenting the volume change per transect, the volume change in each coastal cell is also presented. These results provide a better description of sediment gains and/or losses within a cell and thus of the sediment budget of a larger coastal system. Volume changes are estimated for each coastal cell based on similarities in morphological behavior. This study adopts the method of van Rijn (1997) that divides the part of the North-Holland coast in this study into eight coastal cells (Figure 1). Zone I includes three cells, 1, 2, and 3, in which cell 1 (0 to 8.1 km) is located near the city of Den Helder; cell 2 (8.1 to 16.3 km) is located between Julianadorp and Callantsoog; and cell 3 comprises the area between 16.3 and 20.5 km. Zone III includes five cells, 4, 5, 6, 7, and 8. Cell 4 comprises the area between 26 and 28 km. Cell 5 includes the area between 28 and 39 km. Cell 6 includes the area between 39 and 47 km. Then the last two cells located near IJmuiden harbor are 7 (47 to 50 km) and 8 (50 to 55 km). Volume changes for each coastal cell are estimated by summing the volume changes of all transects in each cell.

Deriving the Accuracy of SDSs, SDSCRs, and SDVCs

For assessing the accuracy of the satellite techniques, this study assumes that the observed JARKUS shoreline provides the ground truth. The horizontal bias of the SDS relative to the JARKUS shoreline is taken as representative for the accuracy. This bias has a positive value if the SDS is found seaward of the JARKUS shoreline or negative if found landward. The test was conducted on a set of 13 images divided into two segments, Zone I and Zone III. Statistical parameters such as maximum landward bias, maximum seaward bias, mean bias, SD, and root mean square error (RMSE) are used to analyze the accuracy in shoreline-change rate of the SDS. A correlation coefficient (R^2) was used to assess the accuracy of SDSCR. The SDs and RMSE are also used to analyze the accuracy in SDVC.

RESULTS

This section first presents the results of the quantitative evaluation of the SDSs. Second, the results of the quantitative evaluation of the SDSCR are presented. Third, the results are presented of the quantitative evaluation of the SDVCs.

Quantitative Evaluation of the SDS

Tables 2 and 3 summarize the SDS error statistics (mean bias, SD, maximum seaward bias, maximum landward bias, and RMSE) obtained for each period analyzed in Zones I and III. The mean bias is obtained by spatially averaging each transect's bias. For Zone I, the annual mean bias between SDS and JARKUS ranges from –3.6 m to 21.3 m, approximately one-half to one pixel size (15 m ÷ 30 m) with a temporal average of 8.1 m over the 25-year period. For Zone III, the annual mean bias ranges largely from –24.6 m to 27.6 m, with an average of 9.2 m over the 25-year period. In general, for the TM images, the mean bias is positive, whereas the mean bias of the ETM+ images (1999 and 2000) is negative. This means that the SDS position of the TM images is generally found seaward of the JARKUS position, while the position of Landsat ETM+ is generally found landward. The recent studies of Pardo-Pascual *et al*. (2012, 2018) also mentioned different type of images (or different sensors) and different spectral resolutions to have significant effects on extracting the shoreline position.

The SD is stable over time and has an average of 11.2 m and 18.5 m corresponding to Zone I and Zone III, respectively. The

Table 2. *Summary of errors of all transects after the application the methodology to Landsat images in Zone I.*

Year	Maximum Landward Bias (m)	Maximum Seaward Bias (m)	Mean Bias (m)	Standard Deviation (m)	RMSE (m)	Total Number Transects
1985	–63.02	25.52	1.86	13.85	13.98	94
1986	–35.39	32.38	6.96	11.23	13.21	94
1987	–38.35	68.02	8.73	10.98	14.03	112
1988	–59.39	27.50	2.31	12.09	12.31	112
1989	–61.26	26.65	2.75	13.33	13.61	112
1990	–27.22	39.01	17.50	10.01	20.16	112
1998	–30.15	36.24	8.46	8.63	12.09	112
1999	–76.91	35.57	–3.61	14.81	15.24	112
2000	–33.22	40.41	4.32	12.78	13.49	112
2005	–5.56	37.27	12.78	8.57	15.39	112
2006	–6.33	49.30	21.28	8.61	22.95	112
2009	–12.48	58.47	15.84	11.37	19.50	112
2010	–14.65	27.36	6.23	8.94	10.90	112
Mean	–35.69	38.75	8.11	11.17	15.14	109

Table 3. *Summary of errors of all transects after the application the methodology to Landsat images in Zone III.*

Year	Maximum Landward Bias (m)	Maximum Seaward Bias (m)	Mean Bias (m)	Standard Deviation (m)	RMSE (m)	Total Number Transects
1985	–35.38	22.94	0.24	12.25	12.26	120
1986	–56.09	23.23	0.20	13.84	13.84	120
1987	–50.52	31.34	6.35	12.00	13.58	121
1988	–80.40	43.15	2.18	35.15	1.48	121
1989	–93.72	60.53	10.82	25.65	27.83	121
1990	0.95	63.01	24.52	10.84	26.81	121
1998	–14.88	67.96	18.51	17.03	25.16	121
1999	–68.69	72.20	1.92	26.68	26.75	121
2000	–114.47	13.53	–24.63	26.90	36.47	121
2005	–8.39	51.82	16.01	13.56	20.98	121
2006	–20.39	73.35	27.64	14.58	31.25	121
2009	–17.10	80.90	18.96	15.61	24.56	121
2010	–17.08	69.13	16.88	16.22	23.41	121
Mean	–44.32	51.77	9.20	18.49	21.88	121

RMSE is stable over time and has an average of 15.1 m and 21.9 m, corresponding to Zone I and Zone III, respectively.

The bias of SDS varies along the length of each zone (Figures 7 and 8). The greatest variation in bias along the shoreline was observed in Zone III, around transect 280 to transect 293 and was found in the years 1988, 1989, 1999, and 2000. Consequently, the SD for these years is higher and ranges from 25.6 m to 35.2 m.

Quantitative Evaluation of the SDSCR

The results of the SDSCR assessed at two different zones and over five different periods averaged over all transects are given in Figure 9 and Tables 4 and 5. The calculations were divided into five different time spans (1985–90, 1990–2000, 2000–10, 1990–2010, and 1985–2010).

The results obtained for SDSCRs from JARKUS and SDS data are shown in Table 4 and Figure 9. In general, both JARKUS and SDS data show much change in shoreline position between 1985 and 1990 with an average accretion rate of 3.1 m/y (JARKUS) and 5.8 m/y (SDS) in Zone I and with an average accretion rate of 3.1 m/y (JARKUS) and 8.8 m/y (SDS) in Zone III. For the other periods, 1990–2000, and 2000–10 the shoreline trends in both JARKUS and SDS data indicate fewer regular changes in accretion and erosion. For the long-term period, 25 years (1985–2010), the shoreline change shows accretion in both datasets, JARKUS and SDS with a similar average rate of 1.2 m/y (JARKUS) and 1.1 m/y (SDS) in Zone I and of 1.6 m/y (JARKUS) and 1.7 m/y (SDS) in Zone III. In general, the SDSCR show a better agreement in both Zones I and III for the period of 25 years (1985–2010). This observation is supported by the derived SDs and RMSE that decrease with increasing time intervals (see Table 5). The highest SD and RMSE are observed in a period of 5 years (1985–90), while the lowest SD and RMSE are found in a period of 25 years (1985–2010). Moreover, the SDSCR within the period 1990–2010 and 1985–2010 show a higher correlation coefficient ($R^2 > 0.77$), while a lower correlation coefficient ($R^2 < 0.69$) is observed in the cross-correlation of the other periods (1985–90, 1990–2000, and 2000–10).

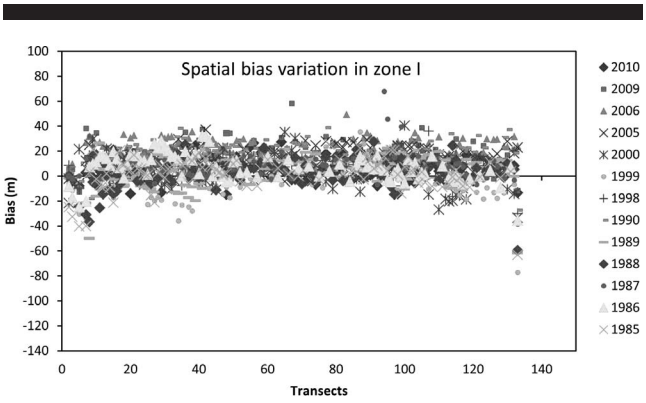

Figure 7. The bias along the shoreline through the years 1985 to 2010 in Zone I. (Color for this figure is available in the online version of this article.)

Quantitative Evaluation of the SDVCs

The results of SDVC along the coast are shown in Figure 10 and Tables 6 and 7. Overall, both JARKUS and SDVC show much change in volume over the period 1985 and 1990. During that period, the SDVC varies between -8.8×10^3 m^3/y to 180.8×10^3 m^3/y with an average of 29×10^3 m^3/y over Zone I (Table 6). In the period 1990 to 2000, both JARKUS and SDVC also show irregular changes in volume along the coast in both zones. Mean volume changes of SDVC indicate negative values (-4.0×10^3 m^3/y [Zone I] and -8.9×10^3 m^3/y [Zone III]), while mean values of JARKUS data show positive values (5.3×10^3 m^3/y [Zone I] and 5.9×10^3 m^3/y [Zone III]). In the other periods, 2000–10, 1990–2010, and 1985–2010, the mean values of volume change in both data sets show positive values.

Table 7 summarizes the SDVC error statistics (mean error, SD, and RMSE) obtained for each period analyzed in Zones I and III. The largest differences in volume changes between the JARKUS and SDVC were found over the 5-year period (1985–90) with highest mean errors varying from 35×10^3 m^3/y (Zone I) and 54×10^3 m^3/y (Zone III). The smallest difference in volume changes were found over the 25-year period (1985–2010) with mean errors varying from 0.4×10^3 m^3/y (Zone I) to 5.8×10^3 m^3/y (Zone III). This observation is supported by the derived SDs and RMSE presented in Table 7. The highest SD and RMSE were found over a 5-year period (1985–90). The smallest SD and RMSE were observed over a 20-year period

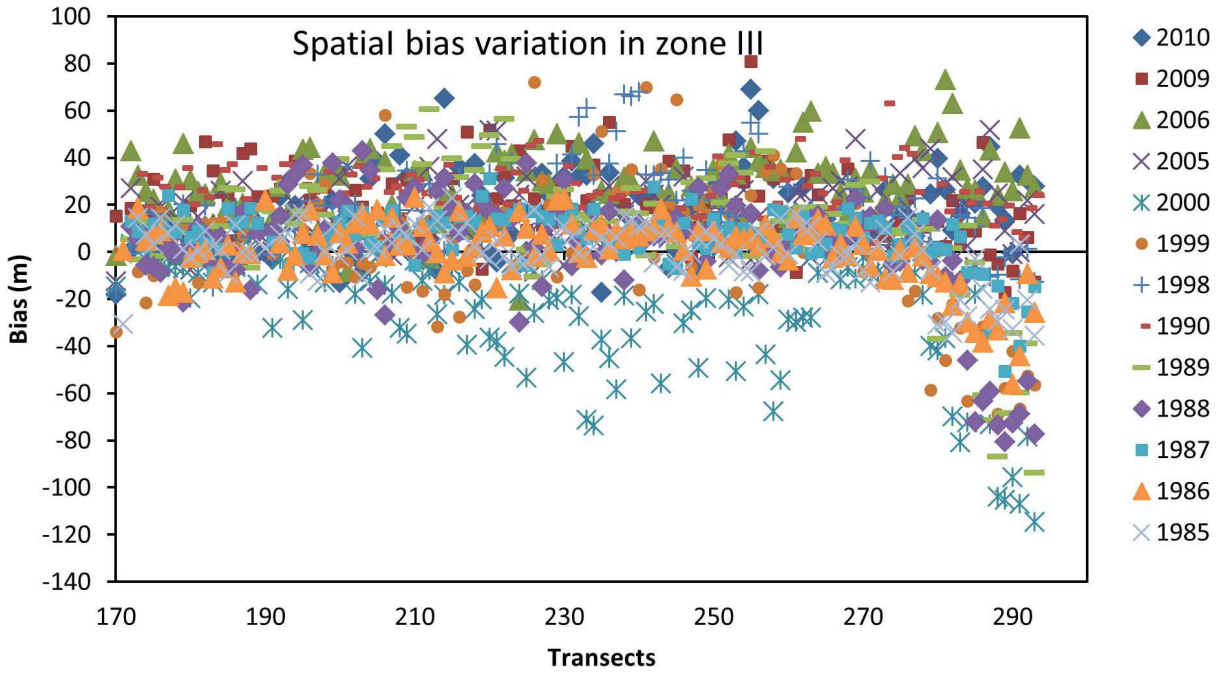

Figure 8. The bias along the shoreline through the years 1985 to 2010 in Zone III. (Color for this figure is available in the online version of this article.)

Table 4. *Summary of results of SDSCR over different periods (1985–90, 1990–2000, 2000–10, 1990–2010, and 1985–2010).*

		1985–90		1990–2000		2000–10		1990–2010		1985–2010	
Zone	SDSCR (m/y)	JARKUS	SDS	JARKUS	SDS	JARKUS	SDS	JARKUS	SDS	JARKUS	SDS
Zone I	Min	–2.17	–1.88	–2.77	–3.11	–4.36	–3.89	–1.14	–1.67	–0.25	–0.53
	Max	13.64	17.43	5.78	2.90	6.84	6.61	3.61	3.09	2.85	2.72
	Average	3.14	5.82	0.69	–0.91	1.15	0.52	0.94	0.51	1.20	1.06
Zone III	Min	–7.89	–0.53	–6.29	–7.20	–6.87	–4.14	–2.36	–2.60	–0.65	–0.35
	Max	13.12	18.03	12.26	5.20	6.39	8.08	6.09	5.15	6.51	6.11
	Average	3.15	8.80	1.67	–1.39	–0.04	2.29	0.80	0.51	1.57	1.67

Table 5. *Summary of errors of SDSCR over different periods (1985–90, 1990–2000, 2000–10, 1990–2010, and 1985–2010).*

	Mean Error (m/y)		Standard Deviation (m/y)		RMSE (m/y)		R^2	
Periods	Zone I	Zone III	Zone I	Zone III	Zone I	Zone III	Zone I	Zone III
1985–90	2.69	5.59	2.35	2.69	3.57	6.20	0.5626	0.5728
1990–2000	–1.60	–3.06	1.27	2.32	2.05	3.84	0.3807	0.5634
2000–10	–0.63	2.35	1.43	2.00	1.56	3.09	0.6417	0.5046
1990–2010	–0.43	–0.30	0.48	0.72	0.64	0.78	0.8299	0.7987
1985–2010	–0.14	0.10	0.32	0.46	0.35	0.47	0.7749	0.8968

Table 6. *Summary of results of SDVC over different periods (1985–90, 1990–2000, 2000–10, 1990–2010, and 1985–2010).*

		1985–90		1990–2000		2000–10		1990–2010		1985–2010	
Zone	SDVC (10^3m3/y)	JARKUS	SDS	JARKUS	SDS	JARKUS	SDS	JARKUS	SDS	JARKUS	SDS
Zone I	Min	–64.38	–8.81	–5.63	–15.75	–2.23	–17.14	–0.37	–8.28	–0.88	–2.34
	Max	33.60	180.86	38.86	13.44	34.14	29.50	20.95	13.79	10.14	10.62
	Average	–5.45	29.12	5.27	–4.05	12.17	2.64	8.05	2.28	4.43	4.79
Zone III	Min	–25.67	–3.02	–53.45	–53.75	–16.09	–32.08	–6.85	–17.29	–6.22	–2.16
	Max	92.71	162.83	31.50	36.37	23.10	60.55	43.33	32.63	22.28	39.15
	Average	1.53	55.50	5.89	–8.92	3.68	15.61	5.86	3.38	4.55	10.38

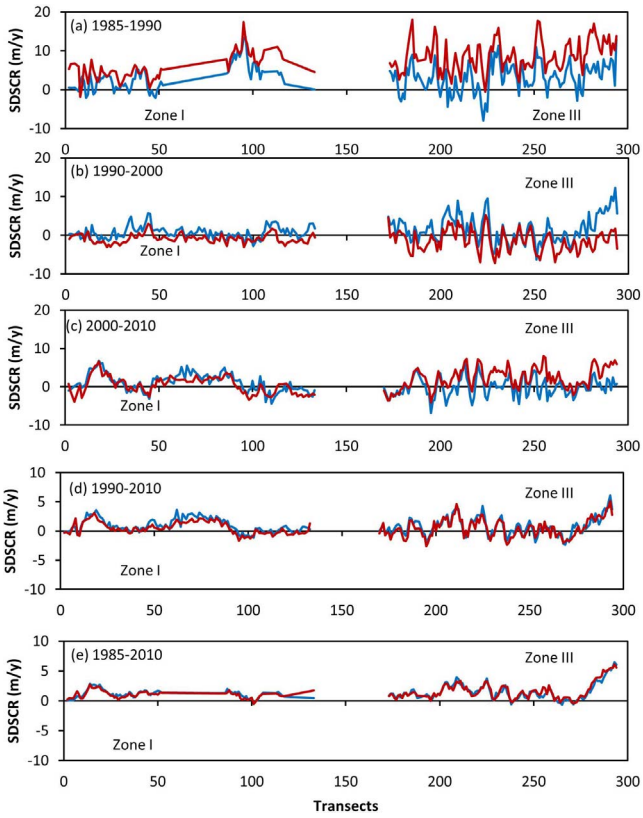

Figure 9. Results of calculated shoreline changes during (a) 1985–89, (b) 1990–2000, (c) 2000–10, (d) 1990–2010, and (e) 1985–2010. The blue lines are shoreline changes from JARKUS, and the red lines are shoreline changes from SDSCR. (Color for this figure is available in the online version of this article.)

(1990–2010) and over a 25-year period (1985–2010). Over the 25-year period, RMSE of SDVC are ranging from 2.5×10^3 m^3/y (Zone I) to 7.7×10^3 m^3/y (Zone III).

Figure 11 shows the volume changes of each cell for both JARKUS and SDVC for different periods. The volumes of each cell are calculated by summing all transect values of each cell. The blue columns indicate the volume derived from JARKUS, while the red column indicates the volume derived from SDVC. For the period 1985–90 (Figure 11a) and the period 1990–2000 (Figure 11b), the SDVCs show many differences in trends and magnitudes of the volume compared with the volume derived from JARKUS. For the other periods (2000–10 [Figure 11c] and 1990–2010 [Figure 11d]), general trends in SDVCs are quite similar compared with volume trends of JARKUS, both indicating that almost all coastal cells are accreting. However, the magnitudes of the SDVC in some cells are underestimated or overestimated compared with JARKUS. For instance, in Figure 10c all cells in Zone I, the SDVC underestimates volumes while the other three cells (6, 7, and 8) in Zone III overestimate the volumes. For the period 1985–2010 (a 25-year period), the SDVCs show a good agreement in both trends and magnitudes, especially for the first four cells in Zone I (Figure 11e). It seems the SDVCs show a better result over long-term periods (over 25 years) than the short-term periods (5 years to 10 years).

DISCUSSION

The comparison between satellite data and JARKUS data over different periods provides a better understanding of the capabilities of using satellite images in shoreline identification

Table 7. *Summary of errors of SDVC over different periods (1985–90, 1990–2000, 2000–10, 1990–2010, and 1985–2010).*

	Mean Error (10^3 m^3/y)		Standard Deviation (10^3 m^3/y)		RMSE (10^3 m^3/y)	
Period	Zone I	Zone III	Zone I	Zone III	Zone I	Zone III
1985–90	34.57	53.97	21.73	30.56	40.84	62.02
1990–2000	–8.99	–14.81	6.51	14.90	11.11	21.01
2000–10	–9.54	11.94	6.90	16.65	11.77	20.49
1990–2010	–5.77	–2.48	3.79	7.25	6.90	7.66
1985–2010	0.37	5.84	2.44	5.03	2.47	7.71

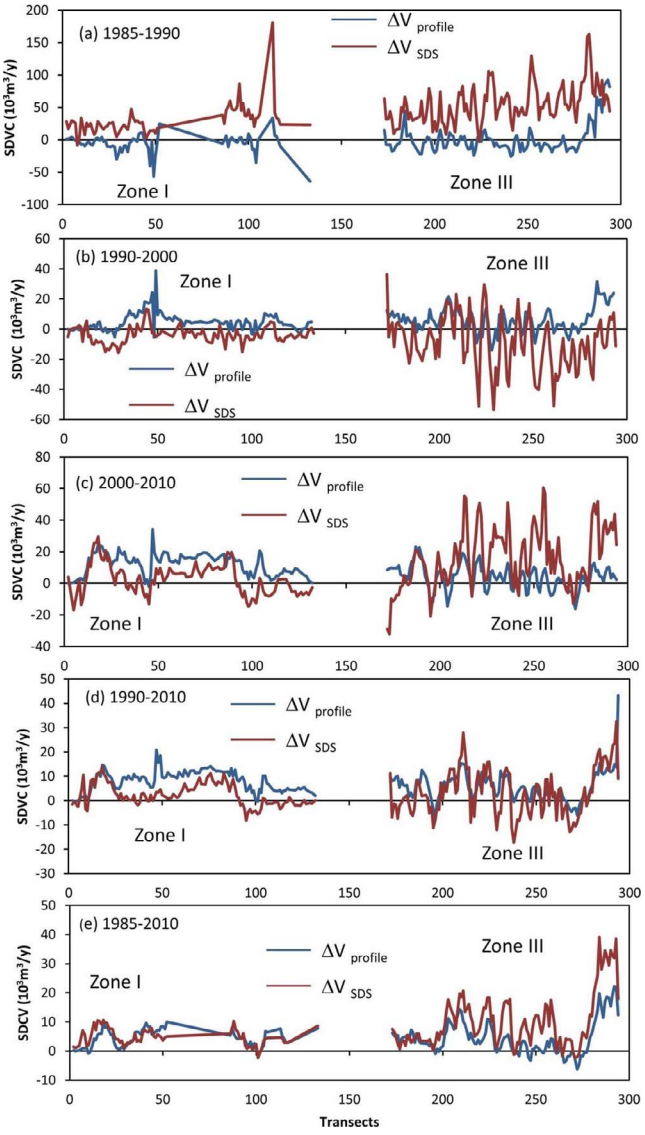

Figure 10. Results of calculated volume changes over different periods (a) 1985–89, (b) 1990–2000, (c) 2000–10, (d) 1990–2010, and (e) 1985–2010. (Color for this figure is available in the online version of this article.)

and shoreline-change rates as well as volume changes. The evaluation revealed that the extracted SDSs at the North-Holland coast have a seaward bias compared to JARKUS measurements of 8.1 m and 9.2 m for Zone I and Zone III. This is in line with current, be it very scarce, literature.

The seaward displacement of SDS relative to the JARKUS shoreline could be explained by light absorption by seawater, and it might vary depending on water transparency (Garcia-Rubio, Huntley, and Russell, 2015). For regions having higher turbidity, perhaps slightly higher wave conditions could increase the seaward displacement. However, the magnitude of these effects is still not known and needs further research. Very recently, Pardo-Pascual *et al*. (2018) evaluated the accuracy of shoreline position obtained from Landsat 7, Landsat 8, and Sentinel-2 imagery on a natural beach and in a port in Valencia, Spain. The results indicate variability brightness in the terrestrial zone influences shoreline detection, brighter zones cause a small landward bias while darker zones move them seaward.

The results of shoreline-change rates indicate a better agreement between the JARKUS and the SDS over longer periods (20–25 years) compared to shorter periods (5–10 years). The smallest SD and RMSE were found over a 25-year period (Tables 4 and 5). The SD and RMSE values increase with a decreasing period. Moreover, the highest RMSE values were found for Zone III in the region near IJmuiden harbour having a large intertidal width. In terms of the correlation coefficient (R^2), the SDSCR shows a strong relationship ($R^2 > 0.78$) over the periods 1990–2010 and 1985–2010 (Table 5). These high values mean that the SDSCR can be used better to quantify the beach change trends over a 25-year period than over shorter periods (5–10 years). The SDSCR methodology can be used to derive shoreline-change rates comparable to those derived from JARKUS. On the other hand, lower regression coefficients values ($R^2 < 0.7$) are observed in the cross-validation of SDSCR over shorter periods (5-year period), indicating more uncertainty of SDSCR over the shorter periods. Probably, the longer periods rely on more data points and thereby averaging the short-term variability in shoreline position leading to more reliable results. This could explain why the SDSCR has better results over periods of 20 years to 25 years than those results obtained over a 5-year period. Almonacid-Caballer *et al*. (2016) suggest using annual mean shoreline positions extracted from Landsat to avoid short-term variability by averaging the instantaneous shoreline positions registered during the same year. Additionally, a larger time scale means larger absolute shoreline changes and thus a larger signal-to-noise ratio. This is clearly indicated in transect 290 (corresponding to profile 7005400 in Figure 12a); the absolute shoreline change during a 20-year period (1990–2010) is larger than that during a 5-year period (1985–90).

The results of SDVC also indicate better results over a 20-year to a 25-year period when compared to a 5-year period. This is reflected by the smallest mean error, SD, and RMSE. Because the volume changes have been calculated based on the results of the SDSCR, similar results between SDVC and SDSCR are to be expected. Using satellite images to observe shoreline changes and volume changes seems to work better when considering longer periods (over 20 years) than shorter periods. The larger error in estimated volume-change rates over shorter time periods could be explained by highly dynamic variations of the profile shape on the time scale of events (Stive *et al*., 2002). On timescales shorter than a year, dynamic variations of the upper shoreface profile may exist because of seasonal variations, cyclic behavior of bars, and episodic changes (dune erosion). On longer timescales, Bosboom and Stive (2015) observed JARKUS profiles over the period 1964 and 2008, where its measured profile variations remain in a steady envelope. This observation may explain why the results of SDVC over a long-term period yield better results than over a short-term period.

The different trends in calculating volume changes from satellite and JARKUS data occurring in some transects might be explained by changes in profile shape. The SDVC from

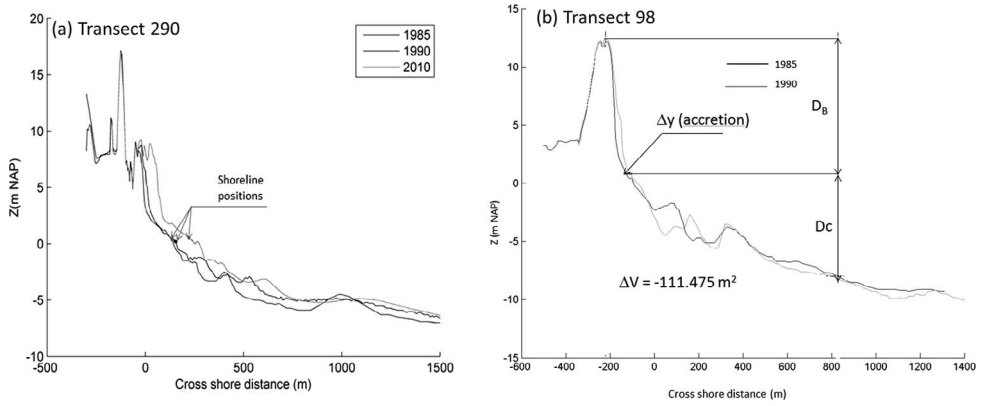

Figure 11. Volume changes through each cell over different periods.

Landsat assumes profiles are static and translated horizontally in seaward and landward direction with accretion and erosion respectively (Figure 5), whereas the JARKUS profiles (Figure 5) do not exactly follow this assumption and changes in profile shape occur. That means that some JARKUS transects show a positive volume change while experiencing shoreline erosion and vice versa (see, *e.g.*, Figure 12b).

To test the validity of the stationary profile assumption, the volume estimated based on shoreline-change rates from the JARKUS data (ΔV_{jarkus} [m^3/y]), were compared with the volume changes that measured from profiles ($\Delta V_{\text{profile}}$ [m^3/y]). Figure 13 indicates the volume-change rates along the coast and the correlation between the JARKUS (ΔV_{jarkus}, blue line), the SDS (ΔV_{SDS}, red line), and the JARKUS profile ($\Delta V_{\text{profile}}$, green line) over the period 1985 and 2010. Figure 13d shows clearly the correlation between the volume changes from the same data but using a different methodology. One is estimated from the shoreline-change rate using the assumption of a static profile, while the other is estimated directly from the measured profile. The dash line indicates the 1:1 regression line, while the continuous line indicates the actual regression line. The correlation analysis shows a significant positive correlation between the $\Delta V_{\text{profile}}$ and the ΔV_{jarkus} ($R^2 = 0.7$). The $\Delta V_{\text{profile}}$ implies a general underestimation compared to the ΔV_{jarkus} with the bigger bias occurring at the higher volume changes. Although the results indicate the correlation is acceptable the cause of the bias could be subject of further research.

This study enables the creation of a quantitative assessment of intertidal zone properties that causes deviation of SDS from JARKUS data. The hypothesis is that the width of the intertidal zone (W) is an important factor in explaining displacement of SDS.

Figure 14 indicates the relationship between the bias (difference between Landsat shoreline position and JARKUS shoreline position) and W. The definition of W is the horizontal distance between the mean high water and mean low water and is estimated from JARKUS profiles. A relationship is investigated between W in terms of pixel size (30 m) and the bias. Consequently, different classes are distinguished where W ranges between one pixel to two pixels ($30 < W \leq 60$ m); W ranges between two pixels to three pixels ($60 < W \leq 90$ m); and W is larger than three pixels ($W > 90$ m). Figure 14 indicates that a gentle beach ($W > 90$ m) and a steep beach ($W \leq 30$ m) show more variation in bias. On wide beaches, this can be explained by the large horizontal range between wet and dry that makes it difficult to identify between land and sea. This observation is similar to the results of the study by Almonacid-Caballer *at al*. (2016). This study has shown that a relation exists between beach slope and the deviation between annual mean shorelines obtained from RTK-GPS and LIDAR surveys

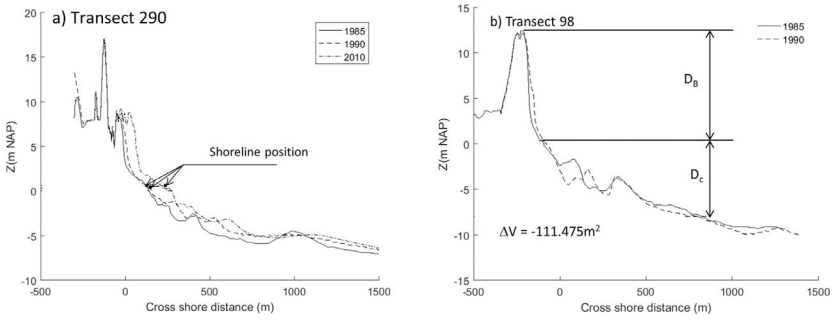

Figure 12. Profile of transect 290 and profile of transect 98 in year 1985, 1990, and 2010.

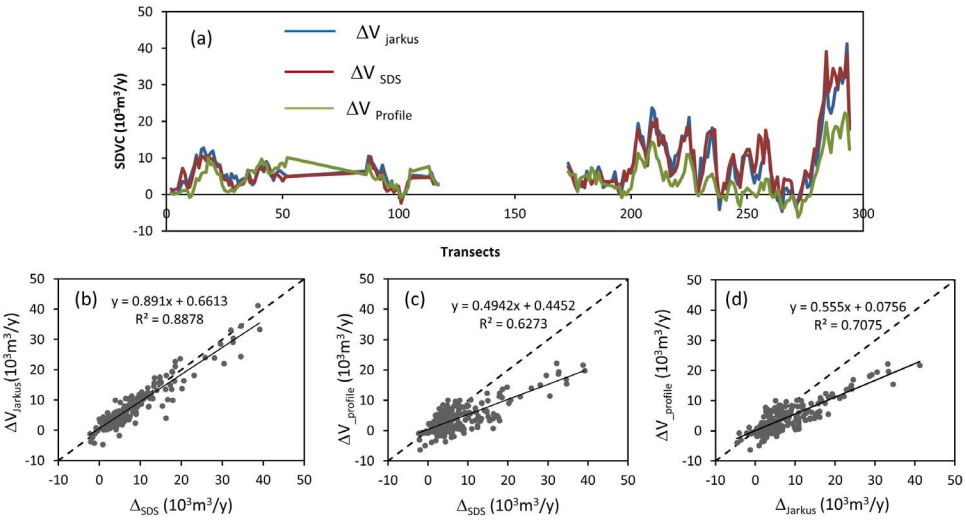

Figure 13. Comparison estimated volume changes and its correlation between derived from SDS, from JARKUS profiles and from shoreline-change rates of JARKUS shorelines. (Color for this figure is available in the online version of this article.)

and Landsat. Their study indicates that shorelines in flatter beach segments are more variable during the year than in steeper segments. For a narrow/steep beach, the classification process between land and water is more sensitive to pixel size in relation to the definition of the shoreline. Steep beaches therefore have also more variation in bias.

Figure 15 also gives the distribution of the bias for different widths (W) of the intertidal zone. The distributions of the bias seem to follow a normal distribution, in which the smallest SD is found in the range of W from one- to two-pixel sizes (Figure 15b). For W less than one-pixel size (Figure 15a) and larger than two-pixel sizes (Figure 15c,d), the distribution of the bias has a larger SD, as illustrated by the wider normal distribution curve (the red curve in the Figure 15). Probably, the derivation of shoreline works best on beaches having intertidal width ranges between one pixel to two pixels ($30 < W \leq 60$ m).

CONCLUSIONS

This study used a combination of satellite remote sensing and GIS techniques for the extraction of SDSs, SDSCR, and SDVC from Landsat images. The accuracy of shoreline extraction was assessed using 13 Landsat 5 TM and Landsat 7 ETM+ images acquired between 1985 to 2010, along two coastal segments of the North-Holland coast. Unsupervised classification was applied using the NDWI to separate sea and land and extract the shoreline from the images. The observed JARKUS shoreline positions derived from the intersection between water level and cross-shore profile at each transect were used to evaluate the error of SDS and SDSCR. The volumes from JARKUS profiles were used to evaluate the accuracy of SDVC.

The evaluation revealed that the extracted SDS at the North-Holland coast has a seaward bias compared to JARKUS

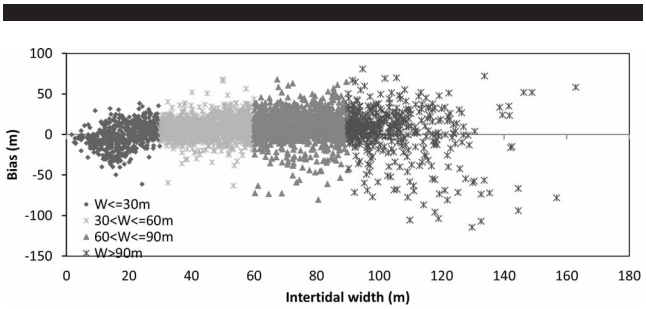

Figure 14. Relationship between intertidal width and bias.

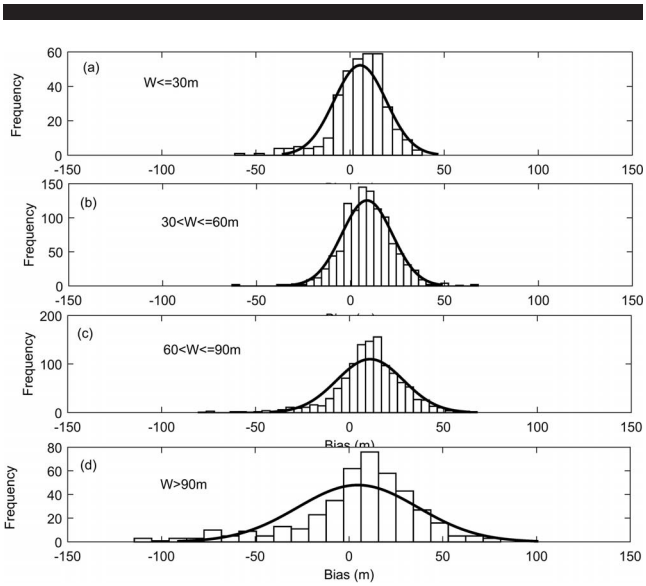

Figure 15. Histogram of errors on intertidal zone widths, with the normal adjusted curve superimposed in black.

measurements of 8.1 m and 9.2 m for Zone I and Zone III, respectively. The mean SD ranges from 11.1 m to 18.5 m and RMSE varies from 15.1 m to 21.8 m. In all cases of Landsat 5 TM, the mean errors tend to indicate a seaward bias, whereas for two Landsat 7ETM images the mean errors are landward.

The results of shoreline-change rates obtained using regression were applied to both datasets, SDS, and JARKUS with five different time periods: a 5-year period (*e.g.*, 1985–90), two 10-year periods (*e.g.*, 1990–2000, 2000–10), a 20-year period (*e.g.*, 1990–2010), and a 25-year period (*e.g.*, 1985–2010). Cross-validation of shoreline-change rate estimations have been performed using statistical techniques, namely, the regression coefficient (R^2) and other statistical parameters such as mean error, SD, and RMSE.

The SDSCRs indicate a better agreement with JARKUS for longer periods (20–25 years) than for shorter periods (5–10 years). The smallest SD and RMSE were found over a 25-year period. The results of the R^2 of the SDSCRs have higher values ($R^2 > 0.78$) over the 20-year and 25-year period. The lower correlation values ($R^2 < 0.7$) are observed in the cross-validation of SDSCR during the shorter periods (5-year period). The finding of smallest mean error, SD, and RMSE and the highest R^2 over the longer period (20 to 25 years) leads to the conclusion that SDSCRs can be derived more successfully over long-term periods than over short-term periods.

Similarly, volume changes obtained from shoreline-change rates indicate less differences when derived from SDS and JARKUS profiles over long-term periods (20 to 25 years) than over short-term period (5 to 10 years).

Finally, the current study has enabled the revelation that the intertidal width (W) influences the accuracy of SDS. The relationship between bias and intertidal beach width indicates that gentle beaches ($W > 90$ m) and steep beaches ($W \leq 30$ m) show more variation in the SDS bias. Interestingly, for beaches that have intertidal beach widths ranging from one- to two-pixel sizes (30–60 m), results obtained are better than for wider or narrower beaches.

In summary, the results obtained suggest the possibility of using Landsat imagery as a source for monitoring shoreline-change rates and volume-change trends over decadal periods. For a short-term period, the results may be influenced by the signal-to-noise ratio and the short-term variations in cross-shore profiles.

ACKNOWLEDGMENTS

This study is part of the Ph.D. of the first author funded through an Erasmus Mundus Mobility Program with Asia (EMMAsia2014) and supported by Delft University of Technology.

LITERATURE CITED

Almonacid-Caballer, J.; Sánchez-García, E.; Pardo-Pascual, J.E.; Balaguer-Beser, A.A., and Palomar-Vázquez, J., 2016. Evaluation of annual mean shoreline position deduced from Landsat imagery as a mid-term coastal evolution indicator. *Marine Geology*, 372, 79–88.

Blodget, H.W.; Taylor, P.T., and Roark, J.H., 1991. Shoreline changes along the Rosetta–Nile Promontory: Monitoring with satellite observations. *Marine Geology*, 99(1–2), 67–77.

Bosboom, J. and Stive, M.J.F., 2015. *Coastal Dynamics I: Lectures Notes CIE4305*. Delft: VSSD, 573p.

Bouchahma, M. and Yan, W., 2012. Long-term coastal changes detection system based on remote sensing and image processing around an island. *2012 Proceedings of 20th International Conference on Geoinformatics* (Hong Kong), pp. 1–5.

Chander, G.; Markham, B.L., and Helder, D.L., 2009. Summary of current radiometric calibration coefficients for Landsat MSS, TM, ETM+, and EO-1 ALI sensors. *Remote Sensing of Environment*, 113(5), 893–903.

Chen, W.-W. and Chang, H.-K., 2009. Estimation of shoreline position and change from satellite images considering tidal variation. *Estuarine, Coastal and Shelf Science*, 84(1), 54–60.

Dinesh Kumar, P.K.; Gopinath, G.; Laluraj, C.M.; Seralathan, P., and Mitra, D., 2007. Change detection studies of Sagar Island, India, using Indian remote sensing satellite 1c linear imaging self-scan sensor III data. *Journal of Coastal Research*, 23(6), 1498–1502.

Du, Z.; Bin, L.; Ling, F.; Li, W.; Tian, W.; Wang, H.; Gui, Y.; Sun B., and Zhang, X., 2012. Estimating surface water area changes using time-series Landsat data in the Qingjiang River Basin, China. *Journal of Applied Remote Sensing*, 6(1), 063609.

Ekercin, S., 2007. Coastline change assessment at the Aegean Sea coasts in Turkey using multitemporal Landsat imagery. *Journal of Coastal Research*, 23(3), 691–698.

Elena, O., 2008. Shoreline and Nearshore Bar Morphodynamics of Beaches Affected by Artificial Nourishment. Universidad Politécnica de Cataluña, Ph.D. dissertation, 103p.

Environmental Systems Research Institute (ESRI), 2014. ArcGIS Desktop Help 10.2 Geostatistical Analyst. http://resources.arcgis.com/en/help/main/10.2/index.html

Feyisa, G.L.; Meilby, H.; Fensholt, R., and Proud, S.R., 2014. Automated water extraction index: A new technique for surface water mapping using Landsat imagery. *Remote Sensing of Environment*, 140, 23–35.

Foody, G.M.; Muslim, A.M., and Atkinson, P.M., 2003. Super-resolution mapping of the shoreline through soft classification analyses. *IEEE Transactions on Geoscience and Remote Sensing*, 3429–3431.

Frazier, P.S. and Page, K.J., 2000. Water body detection and delineation with Landsat TM data. *Photogrammetric Engineering and Remote Sensing*, 66(12), 1461–1467.

García-Rubio, G.; Huntley, D., and Russell, P., 2015. Evaluating shoreline identification using optical satellite images. *Marine Geology*, 359, 96–105.

Gens, R., 2010. Remote sensing of coastlines: Detection, extraction and monitoring. *International Journal of Remote Sensing*, 31(7), 1819–1836.

Grigio, A.M.; Amaro V.E.; Vital, H., and Diodato, M.A., 2005. A method for coastline evolution analysis using GIS and remote sensing—A case study from the Guamaré City, Northeast Brazil. *In:* Finkl, C.W. (ed.), *The Sun, Earth and Moon,* Special Issue No. 42, pp. 412–421.

Guariglia, A.; Buonamassa, A; Losurdo, A; Saladino, R.; Trivigno, M.L.; Zaccagnino, A., and Colangelo, A., 2006. A multisource approach for coastline mapping and identification of shoreline changes. *Annals of Geophysics*, 49(1), 295–304.

Gutierres, F.; Teodoro, A.C.; Reis, E.; Neto, C., and Costa, J.C., 2016. Remote sensing techniques for the assessment of marine and coastal ecosystems. *In*: Finkl, C.W. and Makowski, C. (eds.), *Seafloor Mapping along Continental Shelves*. Cham, Switzerland: Springer, pp. 69–104.

Hagenaars, G.; de Vries, S.; Luijendijk, A.P.; de Boer, W.P., and Reniers, A.J.H.M., 2018. On the accuracy of automated shoreline detection derived from satellite imagery: A case study of the sand motor mega-scale nourishment. *Coastal Engineering*, 133, 113–125.

Hallermeier, R.J., 1978. Uses for a calculated limit depth to beach erosion. *Proceedings of the 16th International Conference on Coastal Engineering* (Hamburg, Germany), pp. 1493–1512.

Hinton, C. and Nicholls, R.J., 1998. Spatial and temporal behaviour of depth of closure along the Holland coast. *Coastal Engineering*, 2913–2925.

International Panel on Climate Change (IPCC), 2001. Climate change. The IPCC Third Assessment report, Volumes I (The Science Basic), II (Impacts, Adaption, and Vulnerability) and III (Mitigation). Cambridge and New York: Cambridge University Press.

Karsli, F.; Guneroglu, A., and Dihkan, M., 2011. Spatio-temporal shoreline changes along the southern Black Sea coastal zone. *Journal of Applied Remote Sensing*, 5(1), 053545.

Kingston, K.S., 2003. Applications of Complex Adaptive Systems Approaches to Coastal Systems. University of Plymouth, Plymouth, U.K., Ph.D. dissertation, 235p.

Knoester, D., 1990. De morfologie van de Hollandse kustzone (analyse van het Jarkus-bestand 1964–1986). Nota GWAO-90.010, Rijkswaterstaat/Dienst Getijdewateren, Den Haag.

Kraus, N.C. and Rosati, J.D., 1998. Estimation of uncertainty in coastal sediment budgets at inlets. *Coastal Engineering Technical Note IV-16,* U.S. Army Engineer Research and Development Center, Coastal and Hydraulics Laboratory, Vicksburg, Mississippi, 12p.

Kuleli, T.; Guneroglu, A.; Karsli, F., and Dihkan, M., 2011. Automatic detection of shoreline change on coastal Ramsar wetlands of Turkey. *Ocean Engineering*, 38(10), 1141–1149.

Kumar, A. and Jayappa, K.S., 2009. Long and short-term shoreline changes along Mangalore Coast, India. *International Journal of Environmental Research*, 3(2), 177–188.

Lawrence, P.L., 1994. Natural hazards of shoreline bluff erosion: A case study of horizon view, Lake Huron. *Geomorphology*, 10(1–4), 65–81.

Liu, H. and Jezek, K.C., 2004. Automated extraction of coastline from satellite imagery by integrating Canny edge detection and locally adaptive thresholding methods. *International Journal of Remote Sensing*, 25(5), 937–958.

Liu, H.; Wang, L.; Sherman, D.J.; Wu, Q., and Su, H., 2011. Algorithmic foundation and software tools for extracting shoreline features from remote sensing imagery and LiDAR data. *Journal of Geographic Information System*, 3(2), 99–119.

Live Waterbase. http://live.waterbase.nl/waterbase_wns.cfm?taal=en.

Lu, D. and Weng, Q., 2007. A survey of image classification methods and techniques for improving classification performance. *International Journal of Remote Sensing*, 28(5), 823–870.

Maiti, S. and Bhattacharya, A.K., 2009. Shoreline change analysis and its application to prediction: A remote sensing and statistics based approach. *Marine Geology*, 257(1–4), 11–23.

Mason, D.C.; Davenport, I.J., and Flather, R.A., 1997. Interpolation of an intertidal digital elevation model from heighted shorelines: a case study in the western wash. *Estuarine, Coastal and Shelf Science,* 45(5), 599–612.

McFeeters, S. K., 1996. The use of the Normalized Difference Water Index (NDWI) in the delineation of open water features. *International Journal of Remote Sensing*, 17(7), 1425–1432.

Miller, T.L. and Fletcher, C.H., 2003. Waikiki: Historical analysis of an engineered shoreline. *Journal of Coastal Research*, 19(4), 1026–1043.

Minneboo, F.A.J., 1995. Jaarlijkse kustmetingen: Richtlijnen voor de inwinning, bewerking, en opslag van gegevens van jaarlijkse kustmetingen. Rapport RIKZ-95.022, April 1995.

Muslim, A.M.; Foody, G.M., and Atkinson, P.M., 2006. Localized soft classification for super-resolution mapping of the shoreline. *International Journal of Remote Sensing*, 27(11), 2271–2285.

Muttitanon, W. and Tripathi, N.K., 2005. Land use/land cover changes in the coastal zone of Ban Don Bay, Thailand using Landsat 5 TM data. *International Journal of Remote Sensing*, 26(11), 2311–2323.

Noernberg, M.A. and Marone, E., 2003. Spatial-temporal monitoring of the Paranaguá Bay inlet margins using multispectral Landsat-TM images. *In:* Klein, A.H.F.; Finkl, C.W.; Rorig, L.R.; Santana, G.G.; Diehl, F.L., and Calliari, L.J. (eds.), *Proceedings of the Brazilian Symposium on Sandy Beaches: Morphodynamics, Ecology, Uses, Hazards and Management. Journal of Coastal Research*, Special Issue No. 35, pp. 221–223.

Pajak, M.J. and Leatherman, S., 2002. The high water line as shoreline indicator. *Journal of Coastal Research*, 18(2), 329–337.

Pardo-Pascual, J.E.; Almonacid-Caballer, J.; Ruiz, L.A., and Palomar-Vázquez, J., 2012. Automatic extraction of shorelines from Landsat TM and ETM + multi-temporal images with subpixel precision. *Remote Sensing of Environment*, 123, 1–11.

Pardo-Pascual, J.E.; Sánchez-García, E.; Almonacid-Caballer, J.; Palomar-Vázquez, J.; de los Santos, E.P.; Fernández-Sarría, A., and Balaguer-Beser, A., 2018. Assessing the accuracy of automatically extracted shorelines on microtidal beaches from Landsat 7, Landsat 8 and Sentinel-2 Imagery. *Remote Sensing*, 10(2), 326; doi:10.3390/rs10020326

Phinn, S.R.; Menges, C.; Hill, G.J.E., and Stanford, M., 2000. Optimizing remotely sensed solutions for monitoring, modeling, and managing coastal environments. *Remote Sensing of Environment*, 73(2), 117–132.

Pianca, C.; Holman, R., and Siegle, E., 2015. Shoreline variability from days to decades: Results of long-term video imaging. *Journal of Geophysical Research: Oceans*, 120(3), 2159–2178.

Plant, N.G.; Aarninkhof, S.G.J.; Turner, I.L., and Kingston, K.S., 2007. The performance of shoreline detection models applied to video imagery. *Journal of Coastal Research*, 23(3), 658–670.

Rokoni, K.; Ahmad, A.; Selamat, A., and Hazini, S., 2014. Water feature extraction and change detection using multitemporal landsat imagery. *Remote Sensing*, 6, 4173–4189.

Rosati, J.D., 2005. Concepts in sediment budgets. *Journal of Coastal Research*, 21(2), 307–322.

Rosati, J.D.; Gravens, M.B., and Smith, G., 1999. Regional sediment budget for Fire Island to Montauk Point, New York, USA. *Proceedings of Coastal Sediments 99* (Hauppauge, New York, ASCE), pp. 802–817.

Rosati, J.D. and Kraus, N.C., 1999. Formulation of sediment budgets at inlets. Vicksburg, Mississippi: U.S. Army Corps of Engineers, *Coastal Engineering Technical Note*, IV-15, 20p.

Rouse, J.W.; Haas, R.H.; Schell, J.A., and Deering, D.W., 1974. Monitoring vegetation systems in the great plains with ERTS. *Third Earth Resources Technology Satelite-1 Symposium*, NASA SP-351 I, pp. 309–317.

Ruggiero, P.; Kaminsky, G.M.; Gelfenbaum, G., and Voigt, B., 2005. Seasonal to interannual morphodynamics along a high-energy dissipative littoral cell. *Journal of Coastal Research*, 21(3), 553–578.

Sánchez-García, E.; Pardo-Pascual, J.E.; Balaguer-Beser, A., and Almonacid-Caballer, J., 2015. Analysis of the shoreline position extracted from landsat TM and ETM+ imagery. The international Archives of the Photogrammetry, Remote Sensing and Spatial Information Sciences, Volume XL-7/W3. *36th International Symposium on Remote Sensing of Environment*, 11–15 May 2015, Berlin, Germany.

Shen, L. and Li, C., 2010. Water body extraction from Landsat ETM+ imagery using adaboost algorithm. *Proceedings of 18th International Conference on Geoinformatics* (Beijing, China), 18–20 June 2010, pp. 1–4.

Sherman, D.J. and Bauer, B.O., 1993. Coastal geomorphology through the looking glass. *Geomorphology*, 7(1–3), 225–249.

Stive, M.J.F.; Aarninkhof, S.G.J.; Hamm, L.; Hanson, H.; Larson, M.; Wijnberg, K.M.; Nicholls, R.J., and Capobianco, M., 2002. Variability of shore and shoreline evolution. *Coastal Engineering*, 47(2), 211–235.

Stolk, A., 1989. *Zandsysteem kust: Eenmorfologische karakterisering*. Technical report, Ministerie van Verkeer enWaterstaat, GEOPRO.

Teodoro, A.C., 2016. Optical satellite remote sensing of the coastal zone environment—An overview. *In:* Marghany, M. (ed.), *Environment Applications of Remote Sensing*. London, U.K., InTechOpen, pp. 165–196.

Teodoro, A.C.; Gutierres, F.; Gomes, P., and Rocha, J., 2018. Remote sensing data and image classification algorithms in the indentification of beach patterns. *In*: Botero, C.M.; Cervantes, O.D., and Finkl, C.W. (eds), *Beach Managements Tools–Concepts, Methodologies and Case Studies*. Cham, Switzerland: Springer, pp. 57–587.

Thieler, E.R.; Himmelstoss, E.A.; Zichichi, J.L., and Ergul, A., 2009. *The Digital Shoreline Analysis System (DSAS) version 4.0—An ArcGis extension for calculating shoreline change*. U.S. Geological

Survey Open-File Report 2008-1278. Available online at http://woodshole.er.usgs.gov/project-pages/DSAS/version4.

Tyagi, P. and Bhosle, U., 2011. Atmospheric correction of remotely sensed images in spatial and transform domain. *International Journal of Image Processing*, 5(5), 564–579.

USGS (U.S. Geological Survey), 2017. *Earth Explorer*. http://earthexplorer.usgs.gov/.

van Rijn, L.C., 1997. Sediment transport and budget of the central coastal zone of Holland. *Coastal Engineering*, 32(1), 61–90.

van Rijn, L.C.; Ruessink, B.G., and Mulder, J.P.M., 2002. Coast3D-Egmond: The behaviour of a straight sandy coast on the time scale of storms and seasons. *In: Process knowledge and guidelines for coastal management*. EC MAST Project No. MAS3-CT97-0086. Amsterdam, The Netherlands: Aqua, 400p.

Wang, C.; Zhang, J., and Ma, Y., 2010. Coastline interpretation from multispectral remote sensing images using an association rule algorithm. *International Journal of Remote Sensing*, 31(24), 6409–6423.

White, K. and El-Asmar, H.M., 1999. Monitoring changing position of coastlines using Thematic Mapper imagery, an example from the Nile Delta. *Geomorphology*, 29(1–2), 93–105.

Wijnberg, K.M., 2002. Environmental controls on decadal morphologic behavior of the Holland coast. *Marine Geology*, 189(3–4), 227–247.

Wilson, E.H. and Sader, S.A., 2002. Detection of forest harvest type using multiple dates of Landsat TM imagery. *Remote Sensing Environment*, 80(3), 385–396.

Xu, H., 2006. Modification of normalized difference water index (NDWI) to enhance open water features in remotely sensed imagery. *International Journal of Remote Sensing*, 27(14), 3025–3033.

Zuzek, P.J.; Nairn, R.B., and Thieme, S.J., 2003. Spatial and temporal consideration for calculating shoreline change rates in the Great Lakes Basin. *In:* Byrnes, M.R.; Crowell, M., and Fowler, C. (eds.), *Shoreline Mapping and Change Analysis: Technical Considerations and Management Implications. Journal of Coastal Research,* Special Issue No. 38, pp. 125–146.